A variable-director ^{13}C NMR analysis of lyotropic aramide solutions

Julia Grinshtein, Dan McElheny, Veronica Frydman, and Lucio Frydman[a)]
Department of Chemistry, University of Illinois at Chicago, Chicago, Illinois 60607

(Received 6 October 2000; accepted 28 December 2000)

The order and dynamics of two aromatic polyamides in their lyotropic phases were investigated with the aid of variable-director nuclear magnetic resonance (NMR). In these experiments polymers were dissolved in concentrated sulfuric acid and allowed to equilibrate inside the main NMR magnetic field B_0 to yield macroscopically-aligned liquid crystalline solutions. These ordered fluids were then rotated away from equilibrium for brief periods of time, and their natural abundance ^{13}C NMR spectra collected as a function of different angles between the liquid crystalline director and B_0. The resulting spectra showed peaks shifting as well as broadening as a function of the director's orientation, variations that were also found to be concentration- and temperature-dependent. All such changes could be successfully accounted for on the basis of an exchange model involving molecular reorientations of the polymer chains that are occurring in the intermediate NMR time scale. Based on this assumption, the experimental line shapes could be used to extract a detailed description of the macromolecular order and dynamics in these fluids. The former appeared substantially high, and not very different from the one characterizing order in commercial extruded aramide fibers. The latter enabled an estimation of the hydrodynamic radii adopted by the macromolecules in their mesophases, which ended up in close agreement with dimensions recently reported on the basis of small-angle neutron scattering analyses. © *2001 American Institute of Physics.* [DOI: 10.1063/1.1349706]

I. INTRODUCTION

Interest in understanding the behavior of liquid crystalline polymers is driven by both basic and applied considerations.[1–10] From a fundamental standpoint, new features are known to arise when combining the anisotropic properties of liquid crystals (LC) with the macro- and mesoscopic characteristics of polymers. From a technological standpoint, these unusual features have been put to practical use towards the development of a variety of ultrastrong materials exhibiting an increasing number of commercial applications. Among the most successful examples of the latter are the aromatic polyamides, or aramides, main-chain mesogenic polymers that can be processed into high performance fibers with superior tensile, chemical, and thermal stabilities.[11–13] Such processing involves dissolving the aramides at suitable temperatures and concentrations into a lyotropic phase where macromolecules are spontaneously aligned with respect to their neighbors. Bulk alignment is then imposed on these liquid crystalline solutions by external shearing fields, leading to an ordered fluid from which polymer fibers can be coagulated and spun. Absolute sulfuric acid counts among one of the few solvents capable of solubilizing and processing these otherwise intractable, strongly hydrogen-bonded polymers.

In view of these considerations it is not surprising that much attention has been devoted to exploring the temperature, concentration, or molecular weight conditions that promote aramide liquid crystallinity, as well as to understand the statistical mechanics that control these forms of macromolecular order.[14–18] Part of these studies involved the application of a variety of physical techniques to the experimental quantification of molecular parameters within these solutions. Nuclear magnetic resonance (NMR) can play an important role in this regard, as over the decades it has become one of the best established tools for investigating molecular properties both in monomeric LCs[19–21] as well as in polymers.[22–24] Key in enabling many of these studies is the anisotropy of NMR interactions, which when properly analyzed can yield structural and dynamic characteristics. During recent years we have been exploiting some of these features to monitor via natural abundance ^{13}C NMR, the order of aramides in H_2SO_4 solutions as a function of their monomeric structure.[25–27] An example of the features displayed by these experiments is presented in Fig. 1, which compares data recorded for the two aramide polymers poly (*p*-benzamide) (PBA) and poly(*p*-phenylene-2,6-naphthylamide) (PPNA) in their respective isotropic and nematic phases. In the first of these phases fast molecular reorientations average away the anisotropic components of the chemical shift tensors (CSA), resulting in conventional sets of ^{13}C peaks positioned solely on the basis of each site's electronic nature. By contrast peaks arising from molecules in the mesophase are shifted from their isotropic values, as a result of the organization of the aramide macromolecules and of their subsequent alignment parallel to the main external NMR field B_0. To analyze such spectra a well-established model can be adopted, according to which molecules in LC phases tumble fast on the time scale of the CSAs ($\approx 10^4 - 10^5$ Hz) but they no longer do so within an isotropic mean

a)Author to whom correspondence should be addressed: Department of Chemical Physics, Weizmann Institute, 76100 Rehovot, Israel. Electronic mail: lucio@uic.edu

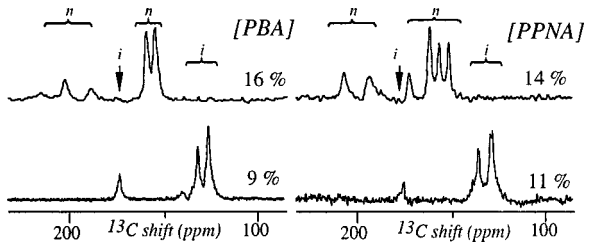

FIG. 1. Concentration dependence of the room temperature ^{13}C NMR spectra recorded for PBA/H_2SO_4 and PPNA/H_2SO_4 solutions. Letters ''*i*'' and ''*n*'' denote signals arising from isotropic and nematic phases, respectively.

potential.[20] This in turn leads to a description of alignment based on the motionally-averaged Saupe ordering matrix $\{S_{ij}\}_{i,j=1-3}$,[28] a second-rank tensor whose principal values can be summarized for uniaxial aramides in terms of a single macromolecular order parameter S_{zz}. We have measured such parameters for a variety of aramide polymers and of sample conditions and, on the basis of an *a priori* knowledge of CSA tensors determined in the solid state, used this information to extract molecular level conclusions about the effects of monomeric structures on the polymers' order.

In spite of its successful account of the ^{13}C spectra we found that this model provides only an approximate description of the lyotropic NMR of aramides. This can be appreciated from Fig. 2(A), which illustrates typical results observed when ^{13}C NMR experiments are collected on any of

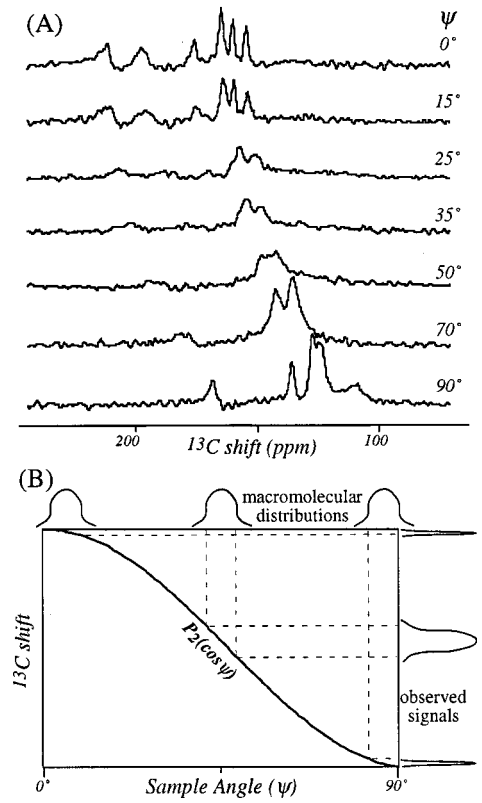

FIG. 2. (A) Variable-director ^{13}C NMR spectra collected on a 14% w/w PPNA solution at the indicated Ψ-values, displaying concurrent shifts and broadenings of the peaks. (B) Rationalization of the experimental variable-director broadenings in terms of incompletely-averaged orientational distributions.

these phases as a function of different orientations Ψ between the nematic director and the magnetic field B_0. According to the classical Saupe model, peak positions in these traces should be given by a rotationally invariant isotropic chemical shift term, plus an anisotropic displacement that scales as $P_2(\cos\Psi)=(3\cos^2\Psi-1)/2$. Such linear $P_2(\cos\Psi)$ dependence of sharp chemically-shifted peaks is routinely observed in LC NMR experiments on low molecular weight nematics, whose directors can be taken away from their natural orientation by means of variable-angle sample spinning.[29] We have also observed a similar behavior in thermotropic polymer experiments where the directors were mechanically taken away from equilibrium for short periods of time with the aid of a stepping motor.[30] Yet in addition to these expected shifts, the aramide/H_2SO_4 spectra in Fig. 2(A) show a clear broadening of the resonances at orientations intermediate between Ψ=0°, 90°.

Such departure from the standard predictions implies that at least one of the model's underlying premises is being violated. In view of the high aspect ratio of the aramides making up the liquid crystal, it is justified to assume that the assumption being broken relates to the rapidness ascribed to the rotational tumbling of the macromolecules with respect to the NMR time scale. Indeed the strong anisometry of rigid aromatic polyamides could lead to a lengthening of their transverse correlation times, to a point that inhibits the averaging of chemical shift anisotropies into sharp motionally-averaged peaks. Each ^{13}C site would then lead to powder-like LC resonances whose line shapes will shift *and* change width as a function of $P_2(\cos\Psi)$, reflecting both the distribution and the dynamics of the macromolecules in the fluid. Broadening effects in such spectra can be expected minimal at Ψ=0°, 90° thanks to the vanishing derivative that P_2 takes at such values [Fig. 2(B)], but substantial at other orientations as is indeed displayed by the actual experiments.

Although coupling a reorientational time scale into the description of aramides' NMR spectra does not invalidate the qualitative conclusions that we have previously derived on the basis of Saupe's model, it complicates the quantitative interpretation of these data. On the other hand the breakdown of the fast-tumbling assumption yields, through a direct analysis of the variable-director line shapes, a sensitive tool to measure not only the ordering but also the dynamics characterizing macromolecules in their fluid phases. Similar effects have actually been observed in the past, particularly in ESR measurements where the large anisotropies that are involved (100's MHz) may bring the reorientational time scales of nonviscous LCs or even of conventional liquids into an intermediate motional regime.[31–33] The potential of variable-director LC experiments has also been demonstrated in the NMR of polymers and membranes, with multiple-pulse analyses of frozen-like systems susceptible to macroscopic rotations by means of mechanical goniometers.[34–37] The application of this strategy to nematic lyotropics such as those made up by the aramide/H_2SO_4 solutions requires slightly modified experimental approaches; such methods, together with the analysis of their spectral data and of the features that they reveal for a variety of temperatures, con-

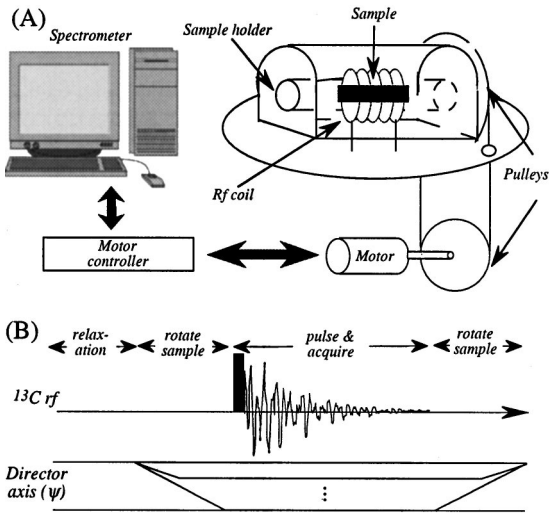

FIG. 3. Experimental setup (A) and pulse sequence (B) employed in the variable-director determinations.

centrations, and monomeric aramide compositions, are described in the following sections.

II. EXPERIMENT

The determinations described in this work focused on two aramide polymers, PBA and PPNA, synthesized as described in Scheme 1.[38]

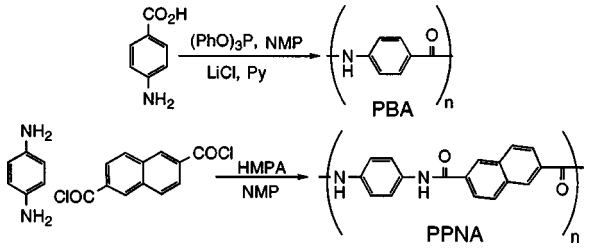

The room-temperature intrinsic viscosities $[\eta]$ measured for these samples in 96% H_2SO_4 were 1.4 and 1.3 dL g^{-1}, respectively. Lyotropic solutions of these polymers were prepared by dissolving suitable sample amounts in freshly-prepared $101\pm1\%$ H_2SO_4. Aliquots of these solutions were then readied for the variable-director NMR experiments by loading them into 5 mm O.D. glass tubes, equipped with a custom square-shaped end that fit tightly into a ceramic pulley. Such pulley was in turn connected via Kevlar® strings to a stepping motor positioned outside the NMR magnet, that defined the orientation of the LC director throughout the acquisition pulse sequence as commanded by the spectrometer's pulse programmer. Natural abundance ^{13}C NMR experiments were recorded on these samples at 75.8 and 50.5 MHz, on laboratory-built spectrometers operating on the basis of a Tecmag® pulse programmer. These machines were equipped with a double-tuned dynamic-director probe containing a free-standing transverse solenoid coaxial with the sample tube [Fig. 3(A)],[30] so that changes in the sample's orientation did not affect its electronic characteristics. The pulse scheme used in the data acquisition is shown in Fig. 3(B); it included an initial equilibration period during which the LC director was allowed to align parallel to the magnetic field B_0, an off-equilibrium period ($\leqslant$150 ms) during which the sample was reoriented away from $\Psi=0°$ and NMR data were collected, and a rotation back to equilibrium in preparation for a new scan. Reorientations were implemented with the aid of a Whedco® PC-interfaced motor controller system, which required approximately 40 ms for turning the LC director by 90°. The actual acquisition of the ^{13}C transients was carried out in the presence of continuous wave (CW) ^1H decoupling (50 kHz rf) using 4 μs $\pi/2$ excitation pulses, 2 s recycle delays, 6000 scans, and no NOE enhancements; such conditions were chosen so that no major distortions in the peak intensities would occur. Temperatures throughout the experiments were stabilized at the desired values using a unit built from Omega® components, and calibrated externally with an ethylene glycol standard. Once collected the NMR data were suitably processed and analyzed on the basis of visual comparisons with spectral simulations. These were calculated on a PC workstation using custom-written C programs developed on the principles described in the following section.

III. THEORETICAL BACKGROUND

As mentioned, the broadenings observed in the variable-director ^{13}C NMR spectra lyotropic polyamides can be ascribed to an incomplete motional averaging of the sites' shielding anisotropies. This implies that the resulting line shapes, particularly at orientations other than $\Psi=0°$ and 90°, will be affected both by the ordering distributions as well as by the rotational dynamics of the macromolecules. To obtain further insight into these parameters a numerical algorithm capable of reproducing the experimental variable-director line shapes was developed. A number of models accounting for such effects have been proposed, particularly by Freed *et al.* in connection to ESR and by Kothe *et al.* in connection to multiple-pulse NMR experiments.[31–37] Several of Kothe's assumptions were adopted for the present study, and adapted to account for the character of the ^{13}C NMR experiments and of the aramide macromolecules.

The starting assumption made was that the overall rotational motions of rod-like macromolecules like the aramides can be described on the basis of two different correlation times: one associated with tumblings perpendicular to the axes of the main-chain ($\tau_\perp^r$), and another linked to reorientations along these main axes $\tau_\parallel^r$. Given the conventional molecular cross sections of the rod-like polymers there are no *a priori* reasons to assume that these longitudinal reorientations will occur slowly with respect to an NMR time scale given by the CSAs (10^4 Hz), and hence the effects observed in the variable-director spectra were ascribed solely to slow ''over-ended'' tumbling motions in the LC. Rather than assuming a continuous diffusive equation for describing these motions, a classical exchange model accounting for dynamics on the basis of lattice jumps was assumed. According to this model (Fig. 4) the spherical coordinates (θ,φ) describing the orientation of a macromolecule inside the fluid are subdivided into a discrete set of $N_\theta \cdot N_\varphi$ equidistant latitudes and longitudes, each associated with a chemical

shift precession frequency $\omega(\theta_i,\varphi_j)$ characteristic for a particular site. The model then assumes that given a certain orientation $|\theta_i,\varphi_j\rangle$ transverse macromolecular tumbling will only proceed to adjacent lattice sites[39]

$$|\theta_i,\varphi_{j\pm1}\rangle \overset{k(\varphi)}{\rightleftharpoons} |\theta_i,\varphi_j\rangle \overset{k(\theta)}{\rightleftharpoons} |\theta_{i\pm1},\varphi_j\rangle, \tag{1}$$

thus mimicking rotational diffusion as a series of successive random walks. The correlation time $\tau_\perp^r$ of the motion is then defined by the first-order exchange rates $\{k(\theta),k(\varphi)\}$, as well as by the angular increment Δ assumed to separate sites in the lattice.

By virtue of the medium's anisotropy and of the polymer's propensity to adopt an ordered distribution inside the NMR magnetic field, the lattice sites will not be equally populated throughout the sphere. This in turn implies that the forward and backward exchange rates between adjacent sites will be orientation-dependent. The axial symmetry of the nematic phases originated by the aramides allows one to assume solely a θ-dependence for the rates and populations, $k=k(\theta_i)$ and $n=n(\theta_i)$, with all the corresponding longitude parameters $\{\varphi_j\}$ equally probable. The kinetic part of the resulting NMR exchange matrix then reads

$$\Gamma=\begin{pmatrix}
 & |\theta_{i-1}\varphi_j\rangle & \cdots & |\theta_i\varphi j-1\rangle & |\theta_i\varphi_j\rangle & |\theta_i\varphi_{j+1}\rangle & \cdots & |\theta_{i+1}\varphi_j\rangle & \\
\vdots & \vdots & \cdots & \vdots & \vdots & \vdots & \cdots & \vdots & \vdots \\
\cdots & -k_\uparrow-k_\downarrow-2k_\leftrightarrow & & 0 & k_\uparrow & 0 & & 0 & \cdots \\
\vdots & \vdots & & \vdots & \vdots & \vdots & & \vdots & \vdots \\
\cdots & 0 & \cdots & k_\uparrow-k_\downarrow-2k_\leftrightarrow & k_\leftrightarrow & 0 & \cdots & 0 & \cdots \\
\cdots & k_\downarrow & \cdots & k_\leftrightarrow & -k_\uparrow-k_\downarrow-2k_\leftrightarrow & k_\leftrightarrow & \cdots & k_\uparrow & \cdots \\
\cdots & 0 & \cdots & 0 & k_\leftrightarrow & -k_\uparrow-k_\downarrow-2k_\leftrightarrow & \cdots & 0 & \cdots \\
\vdots & \vdots & \cdots & \vdots & \vdots & \vdots & \cdots & \vdots & \vdots \\
\cdots & 0 & & 0 & k_\downarrow & 0 & & -k_\uparrow-k_\downarrow-2k_\uparrow & \cdots \\
\vdots & \vdots & & \vdots & \vdots & \vdots & & \vdots & \vdots
\end{pmatrix}
\begin{pmatrix}
|\theta_{i-1}\varphi_j\rangle \\ \vdots \\ |\theta_i\varphi_{j-1}\rangle \\ |\theta_i\varphi_j\rangle \\ |\theta_i\varphi_{j+1}\rangle \\ \vdots \\ |\theta_{i+1}\varphi_j\rangle
\end{pmatrix}. \tag{2}$$

Individual rates in this matrix follow from the principle of detailed balance, according to which a particular $|\theta_i,\varphi_j\rangle$ state can only change under equilibrium conditions at one of three rates:

$$k:\begin{cases}
\langle\theta_i\varphi_j'|k_\leftrightarrow|\theta_i\varphi_j\rangle=\dfrac{k_0}{\sin\theta_n}\delta_{j',j\pm1} \\
\langle\theta_i'\varphi_j|k_\uparrow|\theta_i\varphi_j\rangle=\dfrac{n(\theta_{i'})}{n(\theta_i)}\langle\theta_i\varphi_j|k_\downarrow|\theta_{i'}\varphi_j\rangle\delta_{i',i-1} \\
\langle\theta_{i'}\varphi_j|k_\downarrow|\sigma_i\varphi_j\rangle=(k_0-\langle\theta_{i'}\varphi_j|k_\uparrow|\theta_i\varphi_j\rangle)\,\delta_{i',i+1}.
\end{cases} \tag{3}$$

The total number of lattice sites $N_{\text{total}}=N_\theta\cdot N_\varphi$, coupled to the primary constant k_0 reflecting the rate of the first $\theta_1\rightarrow\theta_2$ reorientation step, provide then an estimate for the over-end rotational correlation times via a comparison with the predictions of Debye's rotational diffusion equation:

$$\tau_\perp^r=\frac{1}{3\Delta^2k_0}. \tag{4}$$

Polar macromolecular populations $n(\theta_i)$ were modeled for these calculations using an orientational distribution function $R(\theta)$, which defines them as[23]

$$n(\theta_i)=\int_{\theta_i-\Delta/2}^{\theta_i+\Delta/2}R(\theta)\,\sin\theta\,d\theta,\quad \Delta=\pi/2N_\theta, \tag{5}$$

and is associated to a liquid crystalline order parameter

$$\langle P_2(\cos\theta)\rangle=\int_0^{\pi/2}R(\theta)\frac{(3\cos^2\theta-1)}{2}\sin\theta\,d\theta. \tag{6}$$

It follows from these arguments that once the $N_\theta\cdot N_\varphi$ lattice dimensions are defined the complete exchange matrix Γ becomes a function of solely two parameters: a rotational correlation time $\tau_\perp^r$, and a LC order parameter $\langle P_2(\cos\theta)\rangle$. The time evolution of ^{13}C magnetizations arising from such model can then be calculated from the Bloch–McConnell differential equations for the transverse magnetization components,

$$\dot{M}_+(\theta_i,\varphi_j)=i\omega(\theta_i,\varphi_j)\cdot M_+(\theta_i,\varphi_j)+\sum_{k,l}\Gamma(\theta_k\varphi_l,\theta_i\varphi_j)M_+(\theta_k,\varphi_l),$$
$$1\leqslant i,k\leqslant N_\theta;1\leqslant j,l\leqslant N_\varphi. \tag{7}$$

In matrix form these equations integrate as

$$\mathbf{M}_+(t)=[\mathbf{D}\cdot\exp(\lambda t)\cdot\mathbf{D}^{-1}]\cdot\mathbf{M_{eq}}, \tag{8}$$

where $\mathbf{M_{eq}}$ is proportional to the equilibrium populations of the lattice points, and $\mathbf{D},\lambda$ are the eigenvectors, eigenvalues of the $i\omega+\Gamma$ matrix. Evaluating the sum of all $M_+(t)$ vector components yields the complete ''powder'' signal for a particular chemical site; suitable addition of all the sites' contributions followed by apodization and Fourier transformation then provides the expected LC ^{13}C spectrum.

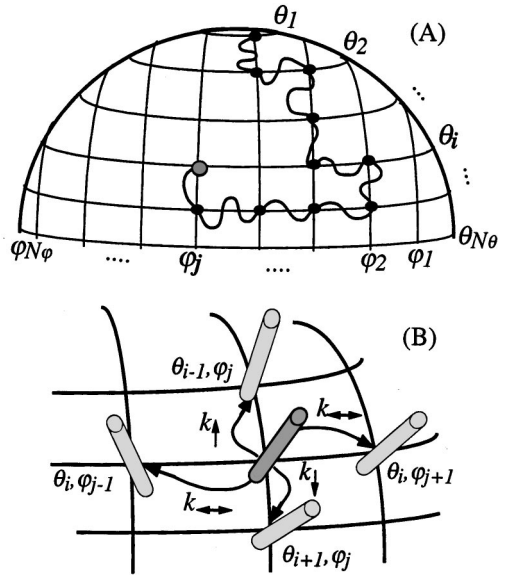

FIG. 4. (A) Lattice model employed for describing the slow transverse molecular tumbling of rigid aramides in their LC solutions. The continuous line represents the trajectory undergone by a unit vector describing a macromolecule's main-chain axis; dots represent those orientations considered by the model. (B) Variations of a generic (θ_i, φ_j) orientation in terms of elementary jumps to neighboring lattice sites.

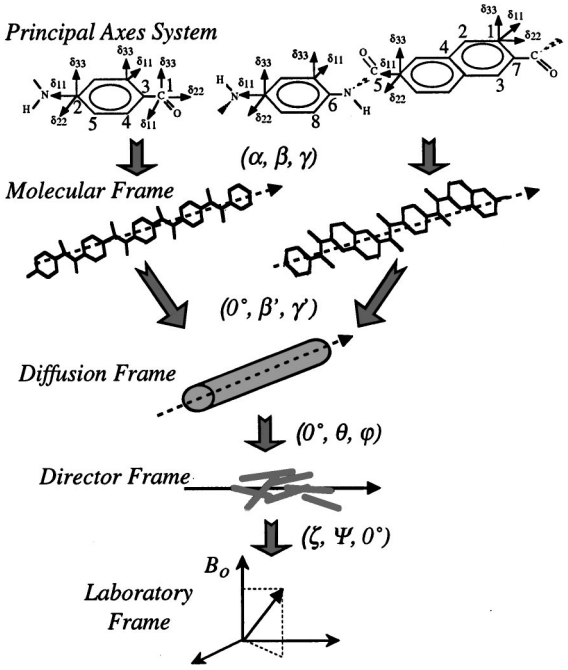

FIG. 5. Euler transformations involved in the calculation of the variable-director ^{13}C frequencies in the laboratory coordinate frame, for any (θ,φ) orientation in the assumed lattice.

The setup of Eq. (7) requires specifying the NMR shielding frequency of a particular chemical site for each point in the spherical lattice. This in turn demands (i) knowledge of the site's chemical shift tensor parameters, (ii) defining the series of second-rank Wigner rotations that shall enable expressing the shifts of the various chemical and lattice sites in a common laboratory frame, and (iii) accounting for all potentially fast motions that are not being explicitly considered by the exchange model of Fig. 4. The basis for defining the chemical shift tensor elements of the sites were the 2D isotropic–anisotropic ^{13}C correlation spectra reported in previous solid state NMR analyses of the polymers.[26,27] For certain sites further modifications of the shielding tensor elements were needed to account for the different isotropic chemical shifts observed in the liqud–crystalline and solid phases; the way by which these differences were established and accounted for are described in the following section. As for the sequence of transformations employed to express the chemical shift tensors throughout the variable-director experiments, these are illustrated in Fig. 5. In addition to Wigner rotations they involve a series of angular averages that account for the fast internal and overall motions that will occur in the LC phase. So for instance after the first transformation from the principal axes system of an individual site to the main symmetry axis of the aromatic ring, an averaging over the γ-angle was introduced to consider the effects of continuous rotations about the ring's axial substituents. A second averaging motion was also added to account for the fast rotation of polymer chains about their main longitudinal diffusion axes, which are slightly tilted from the ring's *para* axes (11° for the PBA and PPNA's diamine rings; 16° for PPNA naphthyl ring).

Before concluding this theoretical survey it is worth summarizing the distinctive effects that the two parameters involved in this numerical model, the degree of mesophasic order $\langle P_2(\cos\theta)\rangle$, and the rate of overall tumbling $\tau_\perp^r$, will have on the variable-director NMR line shapes. As an aid to this end, Fig. 6 illustrates a series of single-site ^{13}C NMR simulations calculated for three orientational distribution functions that were assayed:

$$R = Z\ \exp[-\sin^2\ \theta/2\sigma_\theta^2], \tag{9a}$$

$$R = Z\ \exp[-\sin^2\ \theta/2\ \sin^2\sigma_\theta], \tag{9b}$$

$$R = Z\ \exp[a_2 P_2(\cos\ \theta)], \tag{9c}$$

where Z is a suitable normalization factor, σ_θ are Gaussian broadening factors, and a_2 is a distribution parameter taken from the work of Zannoni.[40] In terms of the actual line shapes all these three $R(\theta)$ functions yielded similar, sensible spectra for a wide range of order and dynamic conditions. The only complications arose when attempting to employ $\exp(-\sin^2\theta/2\sin^2\sigma_\theta)$ to describe systems with low order parameters (with variable-director peaks showing a slight *increase* in the 0°–90° frequency span on decreasing order below some critical value), or when applying the $\exp[a_2P_2(\cos\theta)]$ function to systems with a high degree of order (with a now *decreasing* frequency span for order parameters exceeding ≈0.5–0.6). These limitations were actually to be expected from the assumptions involved in the derivation of these functions; they did not, however, affect the line shapes derived using the $\exp[-\sin^2\theta/2\sigma_\theta^2]$ distribution, which was therefore chosen for matching the actual experimental spectra. Simulations also showed that the resonance's overall excursion upon changing the director's angle Ψ will be mostly influenced by the LC ordering, whereas the extent of the line broadening at intermediate $0°<\Psi<90°$ angles will show a higher sensitivity to the dynamics. This in

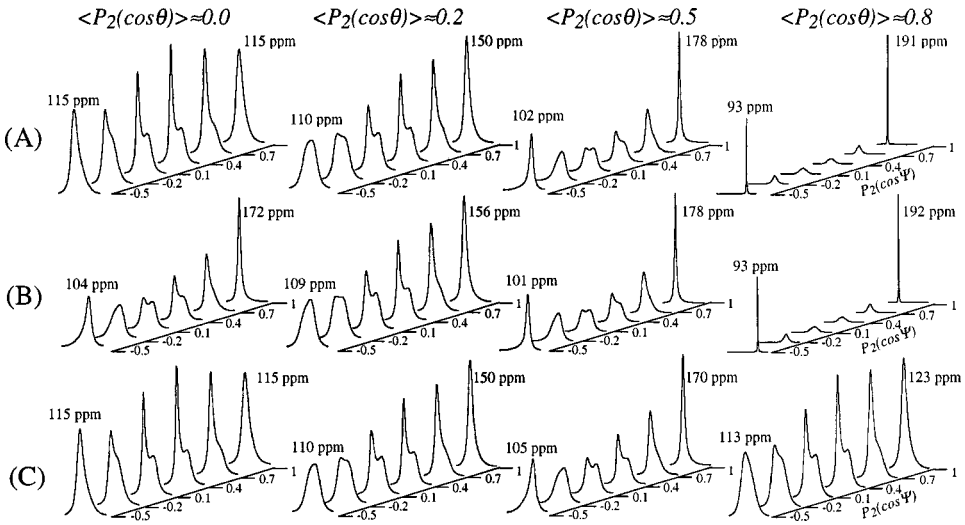

FIG. 6. Variable-director NMR line shapes calculated for different orientational descriptors, with rows (A)–(C) arising from the functions in Eqs. (9a)–(9c), respectively. Also indicated are the approximate peak positions resulting from each model when $\Psi=0°$, 90°. All spectra were computed for a single ^{13}C site with the CSA parameters of PBA's site 2, the indicated order parameters $\langle P_2(\cos\theta)\rangle$, and a tumbling correlation time $\tau_\perp^r=53$ μs.

turn can be understood from the fact that at $\Psi=0°$, 90° orientations the frequency distributions spanned by the $P_2(\cos\Psi)$ scaling factor will be narrow and thus time scales are at their smallest, while at intermediate director orientations it will be the $\tau_\perp^r$ value that will effectively decide whether a site originates a powder-like pattern or a liquid-like resonance.

IV. RESULTS

Figures 7 and 8 compare a series of variable-director ^{13}C NMR spectra recorded on two different PBA/H_2SO_4 solutions, with best fit theoretical simulations derived from the model introduced in the preceding section. Both experimental data sets were acquired at 25 °C but at different polymer concentrations. They differ in the extents of their peak displacements at $\Psi=0°$ and 90° and in the degree of peak broadenings observed at other Ψ orientations, with the most concentrated PBA solution displaying both the largest frequency span as well as the sharpest resonances. These two features are in good agreement with the model described in the previous section: larger variable-director frequency spans will be associated with higher order parameters and thus sharper orientational distributions of the polymer chains; consequently they will possess a smaller CSA-derived time scale and exhibit narrower NMR peaks. In order to quantitatively fit these spectra, Eq. (8) was numerically solved, with the tumbling rates and ordering distributions assumed for the two LC polymer solutions varied until obtaining the optimal simulations displayed at the right of each figure. Both in terms of the peaks' positions and line widths, the agreement observed between both sets of variable-director spectra is very good.

As mentioned, one of the steps involved in calculating these ^{13}C NMR spectra is defining the CSA parameters for

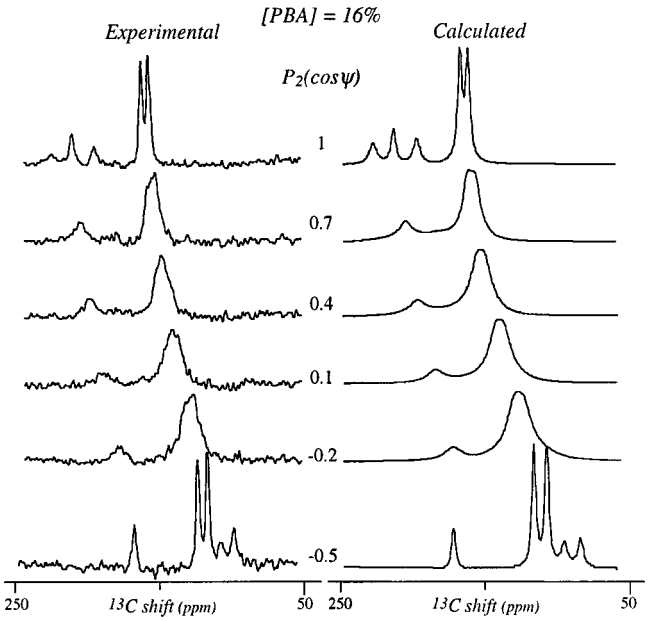

FIG. 7. Experimental vs calculated variable-director ^{13}C NMR spectra recorded at room temperature for a 16% PBA/H_2SO_4 solution. The simulation resulted from the distribution in Eq. (9a) with $\sigma_\theta=8°$, 324 N_{total} lattice sites ($\Delta\theta=\Delta\varphi=10°$), $\tau_\perp^r=53$ μs, the chemical shift parameters in Table I, and a natural line broadening of 200 Hz.

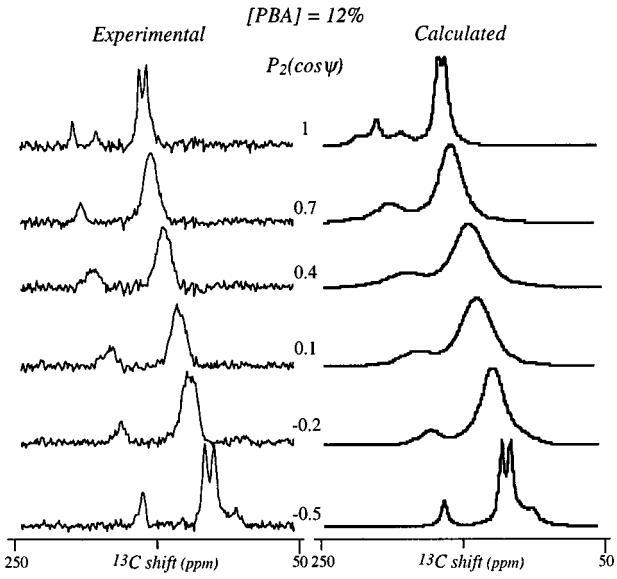

FIG. 8. Same as in Fig. 7 but for a 12% PBA/H_2SO_4 solution. Simulations included $\sigma_\theta=16°$ and other parameters as in the previous figure.

TABLE I. ^{13}C chemical shift tensor values used in the variable-director PBA simulations.[a]

Site	δ_{11} (LC)	δ_{22} (LC)	δ_{33} (LC)	δ_{iso} (LC)[b]	δ_{iso} (solid)[c]	α (deg.)
1	257	166	99	174	166	40
2	255	144	24	141	141	0
3	214	147	17	126	129	0
4	219	162	22	134	127	60
5	207	156	14	126	122	60

[a]In ppm, following the definitions in Fig. 5.
[b]From $\Psi=0°$, 90° dynamic-director measurements.
[c]From CPMAS NMR measurements.

each site. A summary of the principal values and relative orientations assumed for these in the PBA monomer is presented in Table I. The values of the principal tensor elements were based on previous solid state NMR measurements, but had to be modified to account for the isotropic chemical shift differences observed between CPMAS and 2D dynamic-director NMR experiments. The former measure directly these shifts in PBA powdered samples, whereas the latter correlate the lyotropic shifts observed in PBA/H_2SO_4 solutions at $\Psi=0°$ and 90° and therefore extract isotropic displacements from the peak positions,

$$\delta(\Psi=0°)=\delta_{iso}+\delta_{aniso}, \quad \delta(\Psi=90°)=\delta_{iso}-\delta_{aniso}/2. \tag{10}$$

These differences in isotropic shifts vary from -2 to $+6$ ppm depending on the site (Table I), and they are in all likelihood reflecting the site-specific effects of immersing the aramides in such a highly protonating medium as 101% H_2SO_4.[41] On deciding how to modify the solid shielding tensor elements in order to account for these solid/LC shifts, it was found that optimal agreement between simulated sets and variable-director spectra was observed when modifications were ascribed mainly to the δ_{33} components rather than to uniform variations in the tensor elements. This could be rationalized by a protonation-driven change in the electronic densities of the amide groups, which in turn affect the paramagnetic δ_{33} contributions of the aromatic sites due to their conjugation to the $\pi\rightarrow\pi^*$ ring transitions. Finally, the spatial orientations of the CSA tensors were set following well-documented guidelines,[42] which place the most shielded elements perpendicular to the aromatic/amide planes ($\beta=90°$) and the least shielded ones parallel to the aromatic carbon substituents.

Figure 9 compares a series of room temperature variable-director ^{13}C NMR spectra for the PPNA polymer, with best-fit calculations derived from a model similar to the one employed in the PBA simulations. Table II summarizes the chemical shift tensors employed in these data analyses. The basis for the principal elements in this table is again 2D solid state NMR measurements, which due to the monomer's complexity were aided with ancillary measurements on 2,6-naphthyldicarboxyl chloride. Minor differences observed between the isotropic solid and the isotropic LC ^{13}C shifts of the polymer were again accounted for as in the PBA case. Most shielded tensor orientations were uniformly set perpendicular to the aromatic/amide planes, yet best fits of the variable director spectra were obtained when the most deshielded

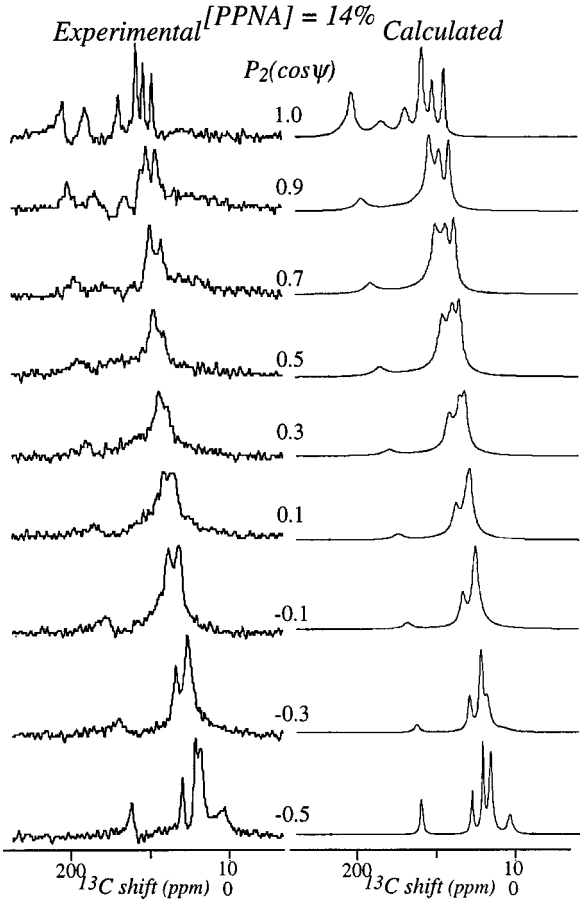

FIG. 9. Same as in Fig. 7 but for a 14% PPNA/H_2SO_4 solution. Simulations involved the parameters in Table II, a Gaussian distribution $\sigma_\theta=19°$, and $\tau_\perp^r=10.6$ μs.

axes of the naphthyl-ring carbon sites were allowed small departures ($\leqslant 10°$) from their ideal orientations. It is not clear whether these have a physical basis or are a reflection of a ''wobbling'' motion that this ring may undergo upon rotating with respect to its 2,6-substitution axes, which are not entirely collinear with the two C–CO chemical bonds.

Variable-director experiments of this kind were also repeated for PBA and PPNA solutions as a function of temperature in an attempt to get insight into the energetics of the molecular tumbling. Figure 10 presents a representative variable-temperature data set recorded for PPNA at a non-equilibrium $P_2(\cos\Psi)=0$ orientation. The line shape varia-

TABLE II. ^{13}C chemical shift tensor values used in the variable-director PPNA simulations.[a]

Site	δ_{11} (LC)	δ_{22} (LC)	δ_{33} (LC)	δ_{iso} (LC)[b]	δ_{iso} (solid)[c]	α (deg.)
1	248	145	−18	125	125	52
2	223	148	28	133	133	52
3	213	138	18	123	133	60
4	202	195	−13	128	132	10
5	258	165	95	172	172	32
6	255	144	24	141	141	0
7	235	113	22	124	133	8
8	211	151	13	125	125	60

[a]Following the definitions in Fig. 5 and in Table I.

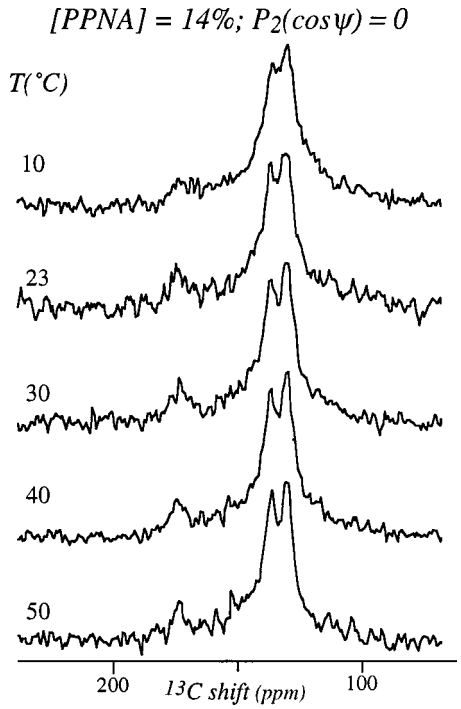

FIG. 10. Variable-temperature ^{13}C NMR spectra collected on a 14% PPNA/H_2SO_4 solution at $P_2(\cos\Psi)=0$. 15 000 scans separated by 1 s delays were collected in each of these experiments.

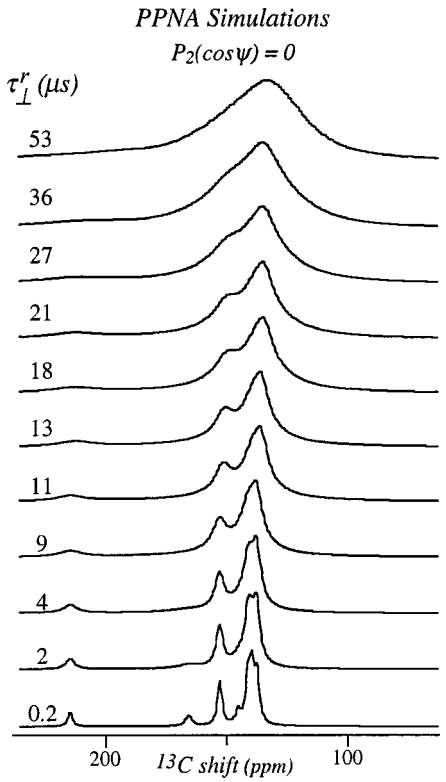

FIG. 11. Simulated set of dynamic NMR data computed to analyze the variable-temperature/variable-director PPNA data. Traces were calculated as in Fig. 9, but for $P_2(\cos\Psi)$ fixed at zero and assuming the indicated transverse correlation times.

tions are not too dramatic, partly as a result of the limited temperature range that can be explored before beginning to decompose the dissolved polymer. Accentuating this constancy is the negligible peak displacements, resulting from a nearly thermal-independent ordering distribution that was already revealed by our previous $P_2(\cos\Psi)=1$ measurements.[26] Yet by contrast to those conventional NMR measurements, the variable-director data reveal an unambiguous and reversible sharpening of the peaks with increasing temperatures arising from enhanced rates of molecular tumbling. Such temperature dependence can be fitted by the Stokes–Einstein relation

$$\tau_\perp^r = 4\pi a r_0^3 \eta/3kT, \tag{11}$$

where η is the viscosity of the solution, and $a^{1/3}r_0$ relates to the rotating solute's effective hydrodynamic radius. By comparing variable-temperature/variable-director spectra with a pool of simulated data (Fig. 11) these rotational correlation times $\tau_\perp^r$ could be estimated, and used to estimate the mean hydrodynamic diameters of the tumbling macromolecules. This entailed measuring the viscosity coefficients for the polymer solutions, and then employ these for extracting $a^{1/3}r_0$ parameters for PBA and PPNA from $\tau_\perp^r$ vs. η/T graphs. A feature that distinguished these viscosity measurements on the polymer solutions over those of pure solvents was their much weaker temperature dependencies. For instance over the $\approx$40 °C temperature range spanned by our experiments $\eta_{H_2SO_4}$ changes by a factor >3, whereas we found aramide solution viscosities varying within $\pm 10\%$ (PPNA) and $\pm 20\%$ (PBA) ranges of their room temperature values. Such behavior agrees with what had been reported by Papkov and co-workers for the viscosities of other PBA solutions, which also observed a weak and nonmonotonic temperature dependence for η.[43] Driven by these considerations it was felt that employing constant viscosities was a justified approximation in deriving the hydrodynamic polymer radii; the $\tau_\perp^r$ vs. η/T plots that then result for PBA and PPNA are summarized in Fig. 12.

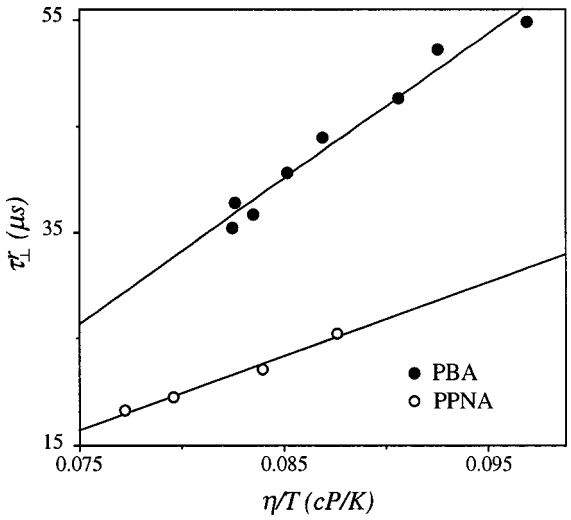

FIG. 12. Stokes–Einstein plots resulting from variable-temperature 16% PBA/H_2SO_4 and 14% PPNA/H_2SO_4 LC NMR spectra. Correlation times $\tau_\perp^r$ result from fitting $P_2(\cos\Psi)$ line shapes; viscosities were estimated from $\eta([c])=\eta_{H_2SO_4}(1+\eta_{inh}\cdot[c])$ as detailed in the text.

TABLE III. Variable-director ^{13}C relaxation times determined of PBA/H_2SO_4 solutions.[a]

Site	T_1 (ms)[b]	$T_{1\rho}$ (ms)[b]
Isotropic	95±15	10±3
Nematic, $\Psi=0°$	63±10	15±3
Nematic, $\Psi=90°$	85±10	15±3

[a]Average of nearly identical values measured for both protonated sites at 25 °C and 35 °C.
[b]From fits of saturation-recovery and spin-lock experiments.

V. DISCUSSION AND CONCLUSIONS

It is clear that from an analytical standpoint variable-director NMR offers a clear molecular-level approach for probing polymeric lyotropic phases. Indeed by largely dissociating the spectral consequences that orientational and dynamic parameters have into position and line shapes factors respectively, this approach bypasses the time scale limitations that may otherwise bias conventional $\Psi=0°$ measurements. As a case in point consider the order parameter gathered for a 16% lyotropic PBA solution using the conventional measurements against that measured for the same system in the present analysis; at room temperature the former was $S_{zz}=0.71$ while from the latter we find $\langle P_2(\cos\theta)\rangle=0.78$. Similar trends are observed for the remaining aramide solutions. This need for modifying the absolute degrees of macromolecular order is a result of the realization that aramide reorientations are not proceeding in the fast tumbling regime usually assumed in LC NMR; respecting the $\Psi=0°$ peak positions while including an explicit dynamic that accounts for the actual NMR time scale then brings about a change in the degree of ordering that needs to be invoked. Still it is worth remarking that the higher degree of alignment for PBA over PPNA and the increase in order with concentrations that were observed at $\Psi=0°$ are also detected by the variable-director experiments.

A question that may arise upon evaluating these data concerns the actual nature of the slow-tumbling entities: are these individual macromolecules as has been considered so far (and as is usually assumed in EPR-related studies),[31,32,34] or are these mesoscopic structures associated for instance to μm-sized defect domains?[44] An answer to this comes from the hydrodynamic sizes derived from the variable-temperature data, which by corresponding to a very small fraction of the sizes expected from domains univocally point to molecular entities. Further evidence for this is provided by the full thermal reversibility detected for the variable-director spectra, a feature that should not characterize domain-driven line shapes because of the susceptibility of these defects to thermal annealing. Yet in an effort to gather one additional independent parameter regarding the rates of molecular tumbling characterizing the anisotropic motion of the macromolecules, ^{13}C relaxation times were measured for the lyotropics when oriented parallel and perpendicular to the magnetic field. The changes observed throughout these $T_1, T_{1\rho}$ relaxation time experiments (Table III) were not significant enough to warrant a modification of the dynamic model introduced above; additional variable-director relaxation measurements with improved *S/N* are currently being pursued on isotopically-labeled samples.

It is possible to further refine the effective hydrodynamic dimensions of the tumbling macromolecules by assuming for them a particular shape. For instance if macromolecules are assumed sufficiently elongated spheroids,[45] ar_0 can be approximated as $2r_0$ and the effective longitudinal radii that result from the plots in Fig. 12 are ~130 and 105 Å for PBA and PPNA, respectively. These dimensions are akin to the 250 Å longitudinal gyration radius recently reported using small-angle neutron scattering for PPTA samples whose M_W were ≈3–4 times larger than those involved in our study,[46] and reinforce again our assumption of a molecular nature for the slow-tumbling entities.

In addition to this size-related insight, it is interesting to remark the high degree of order that the variable-director NMR measurements reveal for the aramides in their lyotropic phases. For instance, a simplistic extrapolation of PBA's 12% and 16% data to the concentration normally used for the spinning of Kevlar® fibers (≈20%) predicts a fluid-phase macromolecular alignment characterized by a sharp $\sigma_\theta\approx5°$ Gaussian distribution. This parameter is not substantially different from the values that have been measured on commercial fibers by means of solid state NMR.[47–49] This would imply that in spite of the extensive manipulations that occur between the dissolution of the aramides into their LC phases and their final processing into fibers, the relative ordering between neighboring macromolecules is not significantly altered. This intriguing possibility is further being explored via a combination of LC- and solid-phase NMR measurements involving fast coagulation of the samples.

ACKNOWLEDGMENTS

We are grateful to Dr. Min Zhou for assistance in the initial stages of this project. This work was supported by the National Science Foundation through Grants DMR-9806810 and CHE-9841790 (Creativity Extension Award), and by the Department of Energy through Grant 00ER15049. L. F. is a Camille Dreyfus Teacher–Scholar, University of Illinois Junior Scholor, Alfred P. Sloan Fellow.

[1] *Liquid Crystalline Order in Polymers*, edited by A. Blumstein (Academic, New York, 1978).
[2] *Polymer Liquid Crystals*, edited by A. Ciferri, W. R. Krigbaum, and R. B. Meyer (Academic, New York, 1982).
[3] E. T. Samulski, Phys. Today **35**, 40 (1982).
[4] M. Gordon and H.-J. Cantou, Adv. Polym. Sci. **59–61** (1984).
[5] *Recent Advances in Liquid Crystalline Polymers*, edited by L. L. Chapoy (Elsevier, Amsterdam, 1985).
[6] H. Finkelmann, Angew. Chem. Int. Ed. Engl. **26**, 816 (1987).
[7] V. N. Tsvetkov, *Rigid Chain Polymers* (Plenum, New York, 1989).
[8] H. H. Yang, *Aromatic High-Strength Fibers* (Wiley, New York, 1989).
[9] *Liquid Crystalline Polymers*, edited by C. Carfagna (Pergamon, Oxford, 1994).
[10] *Liquid Crystalline Polymer Systems*, edited by A. I. Isayev, T. Kyu, and S. Z. D. Cheng (ACS, Washington, 1996).
[11] S. L. Kwolek, P. W. Morgan, J. R. Schaefgen, and L. W. Gulrich, Macromolecules **10**, 1390 (1977).
[12] T. I. Bair, P. W. Morgan, and F. L. Killian, Macromolecules **10**, 1396 (1977).
[13] *Structure and Properties of Oriented Polymers*, edited by I. M. Ward (Chapman and Hall, London, 1997).
[14] S. P. Papkov, Adv. Polym. Sci. **59**, 75 (1984).

[15] T. Odijk, Macromolecules **19**, 2313 (1986).
[16] S. L. Kwolek, P. W. Morgan, and J. R. Schaefgen, *Encyclopedia of Polymer Science and Engineering* (Wiley, New York, 1988), Vol. 9, Chap. 1.
[17] M. G. Northold and D. J. Sikkema, Adv. Polym. Sci. **98**, 115 (1990).
[18] T. Sato and A. Teramoto, Adv. Polym. Sci. **126**, 85 (1996).
[19] Z. Luz, Isr. J. Chem. **23**, 305 (1983).
[20] *NMR of Liquid Crystals*, edited by J. W. Emsley (Reidel, Dordrecht, 1985).
[21] R. Y. Dong, *Nuclear Magnetic Resonance of Liquid Crystals* (Springer, New York, 1997).
[22] V. J. McBrierty and K. J. Packer, *Nuclear Magnetic Resonance in Solid Polymers* (Cambridge University Press, Cambridge, 1993).
[23] K. Schmidt-Rohr and H. W. Spiess, *Multidimensional Solid-State NMR and Polymers* (Academic, London, 1994).
[24] F.A. Bovey and P. A. Mirau, *NMR of Polymers* (Academic, San Diego, 1996).
[25] M. Zhou, V. Frydman, and L. Frydman, J. Phys. Chem. **100**, 19280 (1996).
[26] M. Zhou, V. Frydman, and L. Frydman, Macromolecules **30**, 5416 (1997).
[27] D. McElheny, V. Frydman, M. Zhou, and L. Frydman, J. Phys. Chem. A **103**, 4830 (1999).
[28] A. Saupe, Angew. Chem. Int. Ed. Engl. **7**, 97 (1968).
[29] J. Courtieu, J. P. Bayle, and B. M. Fung, Prog. Nucl. Magn. Reson. Spectrosc. **26**, 141 (1994).
[30] M. Zhou, V. Frydman, and L. Frydman, J. Am. Chem. Soc. **120**, 2178 (1998).
[31] E. Meirovitch and J. H. Freed, J. Phys. Chem. **88**, 4995 (1984).
[32] J. H. Freed, A. Nayeem, and S. B. Ranavare, in *The Molecular Dynamics of Liquid Crystals*, edited by G. R. Luckhurst and C. A. Veracini (Kluwer Academic, Dordrecht, 1994); Chap. 15.
[33] R. Cassol, M.-T. Ge, A. Ferrarini, and J. H. Freed, J. Phys. Chem. B **101**, 8782 (1997).
[34] G. Kothe, Mol. Phys. **33**, 147 (1977).
[35] K. Muller, P. Meier, and G. Kothe, Prog. Nucl. Magn. Reson. Spectrosc. **17**, 211 (1985).
[36] P. Meier, E. Ohmes, and G. Kothe, J. Chem. Phys. **85**, 3598 (1986).
[37] K. Muller, K.-H. Wassmer, and G. Kothe, Adv. Polym. Sci. **95**, 1 (1990).
[38] S. Russo, A. Mariani, V. N. Ignatov, and I. I. Ponomarev, Macromolecules **26**, 4984 (1993).
[39] J. R. Norris and S. I. Weissman, J. Phys. Chem. **73**, 8119 (1969).
[40] C. Zannoni, in *The Molecular Dynamics of Liquid Crystals*, edited by G. R. Luckhurst and C. A. Veracini (Kluwer Academic, Dodrecht, 1994), Chap. 2.
[41] Another possible source of solid/LC differences, relating to differences between the magnetic susceptibilities of the two phases, is made unlikely by the nonuniform magnitudes (and even opposing signs) observed for the solid/LC shifts of the different sites. Because of this consideration we also decided not to include potential anisotropic susceptibility effects in the overall analysis.
[42] J. C. Facelli and D. M. Grant, in *Topics in Stereochemistry*, edited by E. Eliel and S. H. Wilen (Wiley, New York, 1989), p. 1.
[43] S. P. Papkov, V. G. Kulichikhin, V. G. Kalmikova, and A. Y. Malkin, J. Polym. Sci., Polym. Phys. Ed. **12**, 1753 (1974).
[44] Z. Luz and S. Meiboom, J. Chem. Phys. **59**, 275 (1973).
[45] H. Shimizu, J. Chem. Phys. **37**, 196 (1962).
[46] S. J. Picken, L. Noirez, and G. R. Luckhurst, J. Chem. Phys. **109**, 7612 (1998).
[47] R. J. Schadt, E. J. Cain, K. H. Gardner, V. Gabara, S. R. Allen, and A. D. English, Macromolecules **26**, 6503 (1993).
[48] M. Wilhelm, S. F. d. Lacroix, J. J. Titman, K. Schmidt-Rohr, and H. W. Spiess, Acta Polym. **44**, 279 (1993).
[49] J. R. Sachleben and L. Frydman, Solid State Nucl. Magn. Reson. **7**, 301311 (1997).